Digital Alchemy for Materials Design: Colloids and Beyond

Greg van Anders,[†] Daphne Klotsa,[†,‡,§] Andrew S. Karas,[†] Paul M. Dodd,[†] and Sharon C. Glotzer*[,†,⊥,∥]

[†]Department of Chemical Engineering, University of Michigan, Ann Arbor, Michigan 48109-2136, United States, [‡]School of Engineering and Applied Sciences, Harvard University, Cambridge, Massachusetts 02138, United States, [§]Department of Chemistry, University of Cambridge, Lensfield Road, Cambridge CB2 1EW, United Kingdom, [⊥]Department of Materials Science and Engineering, University of Michigan, Ann Arbor, Michigan 48109-2136, United States, and [∥]Biointerfaces Institute, University of Michigan, Ann Arbor, Michigan 48109-2800, United States

ABSTRACT Starting with the early alchemists, a holy grail of science has been to make desired materials by modifying the attributes of basic building blocks. Building blocks that show promise for assembling new complex materials can be synthesized at the nanoscale with attributes that would astonish the ancient alchemists in their versatility. However, this versatility means that making a direct connection between building-block attributes and bulk structure is both necessary for rationally engineering materials and difficult because building block attributes can be altered in many ways. Here we show how to exploit the malleability of the valence of colloidal nanoparticle "elements" to directly and quantitatively link building-block attributes to bulk structure through a statistical thermodynamic framework we term "digital alchemy". We use this framework to optimize building blocks for a given target structure and to determine which building-block attributes are most important to control for self-assembly, through a set of novel thermodynamic response functions, moduli, and susceptibilities. We thereby establish direct links between the attributes of colloidal building blocks and the bulk structures they form. Moreover, our results give concrete solutions to the more general conceptual challenge of optimizing emergent behaviors in nature and can be applied to other types of matter. As examples, we apply digital alchemy to systems of truncated tetrahedra, rhombic dodecahedra, and isotropically interacting spheres that self-assemble diamond, fcc, and icosahedral quasicrystal structures, respectively. Although our focus is on colloidal systems, our methods generalize to any building blocks with adjustable interactions.

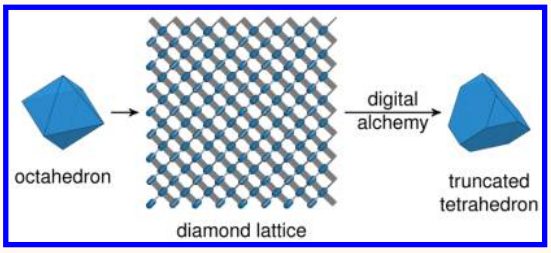

KEYWORDS: digital alchemy · patchy particles · anisotropy dimensions · shape entropy · colloids · materials design · structure–property relationships

Mendeleev's tabular organization of the elements[1,2] by atomic valence[3] has served for more than 140 years as a heuristic that relates properties of the atomic elements to how they arrange in bulk structures. However, attempts to understand how properties of bulk structures relate to atomic properties predate Mendeleev and, in fact, modern science[4] and are complicated by the fact that the chemical manipulation of atoms is prohibited by the quantization of both electrical charge and angular momentum. Fortunately for Mendeleev, this quantization constrains Nature to only about 80 stable elements and limits elemental properties and bulk strutures so that the elements can be tabulated by valence. In fact, starting with technetium[5] in the 1930s, new atomic elements have only been produced artificially (the name technetium comes from the Greek for artificial[6]) by α-particle bombardment, fusion, or other nuclear techniques that finally realized the ancient alchemists' goal of transmuting the elements.

In contrast, an inexhaustible array of new "elements" can be synthesized as patchy particles.[7,8] However, the exploding diversity of patchy particles[8−10] or, more generally, collolidal "elements" means that there are now so many types to synthesize and study that synthesizing them all and determining their bulk structure is no longer possible in practice. This fundamental impracticality means that for colloid science to progress scientists must first ask and answer the basic but daunting question, what elements should I make? Materials science that starts with this question must be carried out in a fundamentally different way than traditional approaches, guided by the question, what is the optimal building block to make for a given structure, and why is it optimal?

* Address correspondence to sglotzer@umich.edu.

Received for review July 7, 2015 and accepted September 24, 2015.

Published online September 24, 2015
10.1021/acsnano.5b04181

Unlike for atoms, colloid valence[11−15] is not discrete. Moreover, entropic colloid valence[14,16] is a collective effect[17] that emerges only when colloids are crowded.[14,16] A first step in identifying a classification scheme for colloidal elements was taken by heuristically classifying building blocks according to their valence along anisotropy dimensions[8,14] that systematically and orthogonally vary colloidal element attributes. This sort of colloidal alchemy is now possible.

Here we present a statistical thermodynamic framework that forms the basis for a new computational approach to building-block design, which we term digital alchemy. Using this framework: (i) We show how to treat anisotropy dimensions[8,14] or other particle interaction parameters as thermodynamic variables and interpret their conjugate quantities. Treating particle interaction parameters thermodynamically means that the attributes of the colloidal "elements" we study can change, so we refer to our methods as "alchemy" in analogy with prescientific attempts to modify chemical elements.[4] The term alchemy has been used previously in the modern era in the context of materials design, and these uses either are different in spirit from the present work[18] or are focused on computing global free energy differences in systems[19,20] in which intermediate state points are unphysical. A related investigation was also carried out in ref 21, which considered the effects of nonrigid colloid shape on crystallization mechanically, whereas here we study rigid colloids that fluctuate thermally. Although there are many systematic investigations of how particle shape or interactions affect structure,[10,14,22−45] we are aware of no work that attempts to directly probe the thermodynamic response of a system to a change in the attributes of its constituent building blocks. (ii) We show how constitutive relations between anisotropy parameters and the thermodynamically conjugate variables we term "alchemical potentials" encode a broad class of detailed quantitative relations between building-block attributes and bulk structure. Further, we define new moduli and susceptibilities that describe stress−strain relationships between bulk structure and particle attributes. (iii) We show that these building block *vs* bulk relationships persist in systems with entropy-driven, emergent collective behavior. (iv) We show how the relation between building block and bulk structure can be used both to determine optimal particle shapes or interactions for given structures and to compute the relative importance of different particle attributes for bulk structure. (v) We report a detailed, general microscopic design rule for a macroscopic, entropy-driven, emergent behavior. (vi) We demonstrate this design rule in simulations that allow particle shape to fluctuate dynamically by showing that when particles are constrained to sit on a target lattice, they spontaneously adopt their preferred shape, *i.e.*, the shape that minimizes the free energy of the target structure at a given state point. Although our main focus is on colloidal systems, our methods immediately generalize to any system with building blocks that have adjustable interactions, *e.g.*, polymers and DNA origami.

Collectively, our findings demonstrate that although atoms and colloids are both usefully classified by valence, in colloidal materials the relationships that exist between particle attributes and bulk structure are very different from the building block *vs* bulk relationships that the periodic table describes for atoms. We show that whereas the periodic table provides information for atomic materials that is complete, but heuristic, for colloidal materials the building block *vs* bulk relationships are incomplete but sufficiently quantitative to both determine optimal building-block attributes for bulk structures and explain why they are optimal.

RESULTS AND DISCUSSION

Theoretical Results. In previous work,[8] Glotzer and Solomon showed how to classify colloidal elements by describing particle valence in terms of anisotropy dimensions. The particle valence encoded in terms of anisotropy dimensions is usually considered to be fixed for any given system. Here, instead of having fixed particle attributes, we allow particle attributes to vary *in situ*. We will allow variation in particle attributes for a given set of particles along all relevant anisotropy dimensions and show that doing so consistently within the framework of statistical mechanics dictates that each particle attribute has a thermodynamically conjugate quantity. We will then show that these thermodynamically conjugate quantities encode detailed information about how building-block attributes affect bulk structure and can be used to deduce optimal building blocks for given structures.

We consider a family of "basic" elements that can be described by a set of isotropic interaction potentials or by anisotropy dimensions for enthalpic[8] or entropic[14] patches, with parameters $\{\alpha_i\}$. Although the focus of the present work is on colloidal systems, the basic elements could be any type of material building blocks that have adjustable interactions. The particles are described by a classical Hamiltonian H that depends on the α_i *via* a pair interaction between particles and the rotational kinetic term in the Hamiltonian

$$H(\{\alpha_i\}) = \frac{p^2}{2m} + \frac{1}{2}L^T I^{-1}_{\{\alpha_i\}} L + U_{\{\alpha_i\}}(q, Q) \qquad (1)$$

where p are momenta, L are angular momenta, I is the moment of inertia tensor, and U is the interaction potential that depends on particle positions q and orientations Q and where we have suppressed particle indices. We consider systems in which the generalized particle coordinates and their conjugate momenta do not have explicit dependence on the α_i. [In this case, the α_i have vanishing Poisson brackets with the

Hamiltonian and are invariants of the system: $\{\alpha_i, H\} = 0$. This is the case if, for example, a particle's shape is independent of its generalized momentum and position. This would not hold, for example, for systems with chemical gradients that cause a particle to swell in some locations more than others. Furthermore, we consider systems in which the α_i themselves are mutually commuting; that is, the order in which operations are applied to modify the building blocks is not important.] We regard the α_i as a set of mutually conserved charges, and it has been shown[46,47] that there is a well-defined thermodynamic ensemble for any set of mutually commuting conserved charges.

Formally, we consider a system where the α_i fluctuate thermally about some averages $\langle\alpha_i\rangle$ and the energy fluctuates about an average $\langle E\rangle$. The partition function for this ensemble can be found with various methods. For brevity we start with the Shannon/Jaynes[48,49] entropy

$$S = -\sum_{\sigma}\left[\pi_\sigma \ln(\pi_\sigma) - \beta(\pi_\sigma H - \langle E\rangle - \sum_i \mu_i N(\pi_\sigma \alpha_i - \langle\alpha_i\rangle))\right] \tag{2}$$

where we have set $k_B = 1$, π_σ is the probability of finding the system in a state labeled σ, β and μ_i are Lagrange multipliers enforcing the thermal averages, N is the number of particles in the system (the factor of N is included here so that both μ_i and α_i can be intensive quantities), and the summation should be interpreted schematically. Also, unless otherwise noted we will work in units where the particle volume $l^3 = 1$. To determine the partition function we maximize eq 2 with respect to π_σ. This gives, up to some normalization constant $\mathcal{Z}$,

$$\pi_\sigma = \frac{1}{\mathcal{Z}} e^{-\beta(H - \sum_i \mu_i N \alpha_i)} \tag{3}$$

and fixing the normalization $\sum_\sigma \pi_\sigma = 1$ gives

$$\mathcal{Z} = \sum_{\sigma} e^{-\beta(H - \sum_i \mu_i N \alpha_i)} \tag{4}$$

We see that $\beta = 1/T$, the usual inverse temperature, and μ_i are thermodynamic quantities conjugate to the α_i. In the physics literature it has become standard practice to refer to all intensive quantities that enter a partition function in a manner similar to, for example, the pressure or chemical potential and do not have pre-existing names as generalized "chemical potentials" (see, for example, refs 46, 47, and 50−52). The generalized chemical potentials that we introduce here correspond not to a change in the number of particles, but rather to a change in building-block attributes. Modifying the properties of the atomic elements was one of the (failed) aims of the ancient alchemists. We thus refer to the generalized chemical potentials we introduce here to modify properties of colloidal "elements" as "alchemical potentials". As we show in this paper, alchemical potentials encode how a system responds to changes in its building-block attributes.

We define the thermodynamic potential for the ensemble in eq 4 as $\mathcal{Z} \equiv e^{-\beta\phi}$, which gives

$$\langle\alpha_i\rangle = -\frac{1}{N}\left(\frac{\partial\phi}{\partial\mu_i}\right)_{N,\eta,T,\mu_{j\neq i}} \tag{5}$$

where η is the packing fraction or density. This computes how the system responds to a change in alchemical potential and in the thermodynamic limit (hereafter we will drop the $\langle\rangle$ notation) establishes a constitutive relation $\alpha_i(\eta,T,\{\mu_j\})$. It is convenient to make a Legendre transformation $F = \phi + \sum_i \mu_i N \alpha_i$ and compute the constitutive relation $\mu_i(\eta,\beta,\{\alpha_j\})$ using the expression

$$\mu_i = \frac{1}{N}\left(\frac{\partial F}{\partial\alpha_i}\right)_{N,\eta,T,\alpha_{j\neq i}} \tag{6}$$

For notational simplicity, especially in cases where we consider a single α_i, it will sometimes be convenient to drop the subscripts on α and μ.

The constitutive relation $\mu(\alpha)$ quantifies the thermodynamic response of a system to a change in the attributes of the constituent particles. If the alchemical potential $\mu > 0$ at some state point $NVT\alpha$, then an infinitesimal increase in the alchemical parameter α would increase the free energy of the system. Conversely if $\mu < 0$, then an infinitesimal increase in α would decrease the free energy of the system. This has two important implications. (i) Locally optimal particle attributes α^* are determined by the roots of the constitutive relation $\mu(\alpha^*) = 0$ with positive slope. We show in the SI that the locations of these roots are invariant under reparametrizations of α. (ii) In hard particle systems, where the free energy simply measures the system entropy, μ directly measures how the number of states available to a system changes as a function of the particle shape, and so it can be used to systematically determine which particle features are most likely to come into contact and provides explicit quantitative guidance on how to design shapes for structures. We demonstrate both of these implications below.

In the next section, we explicitly compute μ in three example systems and interpret the meaning and implications of each computation. We compute the constitutive relation $\mu_i(\eta,T,\{\alpha_j\})$ at $\eta,T,\{\alpha_j\}$ numerically using eq 6 with the Bennett acceptance ratio method.[53] Using this method, we compute μ at some $\{\alpha_j\}$ by equilibrating several independent samples at nearby values $\alpha_j + \nu h_j$, where ν are constants chosen for an appropriate finite differencing scheme and h_j are finite differences. For a full description of the computation, see the SI. To determine the valence for anisotropic particles, we use the potential of mean force and torque (PMFT), as described in ref 16.

In addition to constitutive relations between thermodynamic quantities (*i.e.*, first-order derivatives of the free energy), physical systems are also frequently characterized by higher free energy derivatives: susceptibilities and moduli (see, for example, refs 54 and 55). We define the alchemical modulus M_α and susceptibility χ_α as

$$M_\alpha \equiv \left(\frac{\partial \mu}{\partial \alpha}\right)_{N,\eta,T}, \quad \chi_\alpha \equiv \left(\frac{\partial \alpha}{\partial \mu}\right)_{N,\eta,T} \tag{7}$$

The extension to systems with several alchemical parameters is straightforward. We note that, like standard moduli (*e.g.*, bulk, shear, Young's), M_α is a stress−strain relationship,[55] but the strain is in alchemical space rather than real space. Accordingly, alchemical modulus M_α (eq 7) at α^* measures how sensitive the system is to deviations from the ideal particle properties. Similarly, like standard susceptibilities (*e.g.*, compressibility),[55] χ_α is a strain−stress relationship. Physically,for example, by the fluctuation−dissipation theorem (see, for example, ref 54) χ_α determines how quickly a system of, say, fluctuating shape relaxes when particles are perturbed from their equilibrium attributes.

Numerical Results and Discussion. We use our digital alchemy methodology to optimize building blocks for self-assembly in three different case studies. The first two involve entropy-driven systems, which are among the most conceptually difficult in which to connect macroscopic and microscopic system properties because the macroscopic behaviors are intrinsically collective.[14,16,58−60] In the third study, we investigate an oscillating pair potential, which was recently shown[42] to self-assemble a one-component icosahedral quasicrystal, one of the most complex crystal structures known. In each case, the details of the specific model are included in the discussion below. Details and extended discussion of the methods used in each case may be found in the SI.

Truncated Tetrahedra. We simulated a one-parameter family of truncated tetrahedra at moderate truncations known to self-assemble diamond lattices.[33] We parametrized the truncation between $\alpha = 0$ (a tetrahedron maximally truncated so that it is an octahedron) and 1 (an untruncated, regular tetrahedron). With this parametrization particles self-assembled diamond at a packing fraction of $\eta = 0.6$ between truncations of 0.25 and 0.475 (see Figure 1a; the reparametrization invariance of our results is discussed in the SI). For reference, the Archimedean truncated tetrahedron[33] has a truncation of 1/3. We performed standard Monte Carlo (MC) simulations (*e.g.*, ref 61) of systems of $N = 216$ and 1000 particles at fixed volume. Polyhedra overlaps were checked using the GJK algorithm.[62]

For the truncated tetrahedra, we computed the constitutive relation between vertex truncation α and its conjugate alchemical potential μ. We first computed μ in small systems of $N = 216$ particles and found preliminary evidence for vanishing alchemical potential (here, a free energy minimum) for $0.35 < \alpha^* < 0.4$ (Figure 1d, squares). To obtain higher precision and to test for finite size effects, we simulated systems of $N = 1000$ particles in the region surrounding the putative free energy minimum (Figure 1d, circles). From these alchemical potential computations we extracted the free energy of the system as a function of shape in the vicinity of the minimum (Figure 1d, inset), which we estimated by performing a weighted least-squares fit to

$$\beta\mu = \beta M_\alpha(\alpha - \alpha^*) \tag{8}$$

from which we find the free energy minimum is at

$$\alpha^* = 0.3736 \pm 0.0001 \tag{9}$$

and the alchemical modulus M_α is

$$\beta M_\alpha(\alpha = \alpha^*, \eta = 0.6) = 52.0 \pm 0.3 \tag{10}$$

We also constructed diamond densest packings (Figure 1f) for truncated tetrahedra for all truncations (in increments of 0.001) at which self-assembly into diamond lattices was reported in ref 33 and find the curve has a maximum consistent with the Archimedean truncated tetrahedron at $\alpha_A = 1/3$.

To directly examine the effects of shape modification on emergent valence,[14,16] we computed the PMFT for systems of $N = 1000$ truncated tetrahedra. For details of this computation, see ref 16. We computed the PMFT at a density of $\eta = 0.6$ for a truncation of $\alpha = 0.25$ (Figure 2a) and a truncation of α^* (Figure 2b). The results for the first neighbor shell show particles have stronger tetrahedral valence at α^* than at $\alpha = 0.25$, which originates from the relatively larger hexagonal faces acting as stronger entropic patches.[14] However, we see that at a fluid density of $\eta = 0.5$, in the second neighbor shell when particles have the optimal truncation α^* (cyan spots in Figure 2c), the next-to-nearest neighbors sit in an alternating arrangement, whereas the next-to-nearest neighbors for perfect tetrahedra (blue spots in Figure 2d) are rotated by $\pi/6$. This indicates a nonalternating arrangement that coincides with polytetrahedral motifs not commensurate with the diamond lattice, which arises from steric constraints depicted in Figure 1c. To directly confirm this result, we performed simulations in an $NVT\mu$ ensemble (*i.e.*, both thermostated and "alchemostated") to determine $\alpha(\mu)$ at $\mu = 0$ for $N = 216$ and 1000 truncated tetrahedra with fluctuating shape in a diamond Einstein crystal. We initialized the system at low packing fraction $\eta = 0.2$ with fully truncated (*i.e.*, octahedral, $\alpha = 0$) particles and slowly compressed the system to the target packing fraction of $\eta = 0.6$, after which we relaxed the spring constant. We observed that the process drove the particles to spontaneously

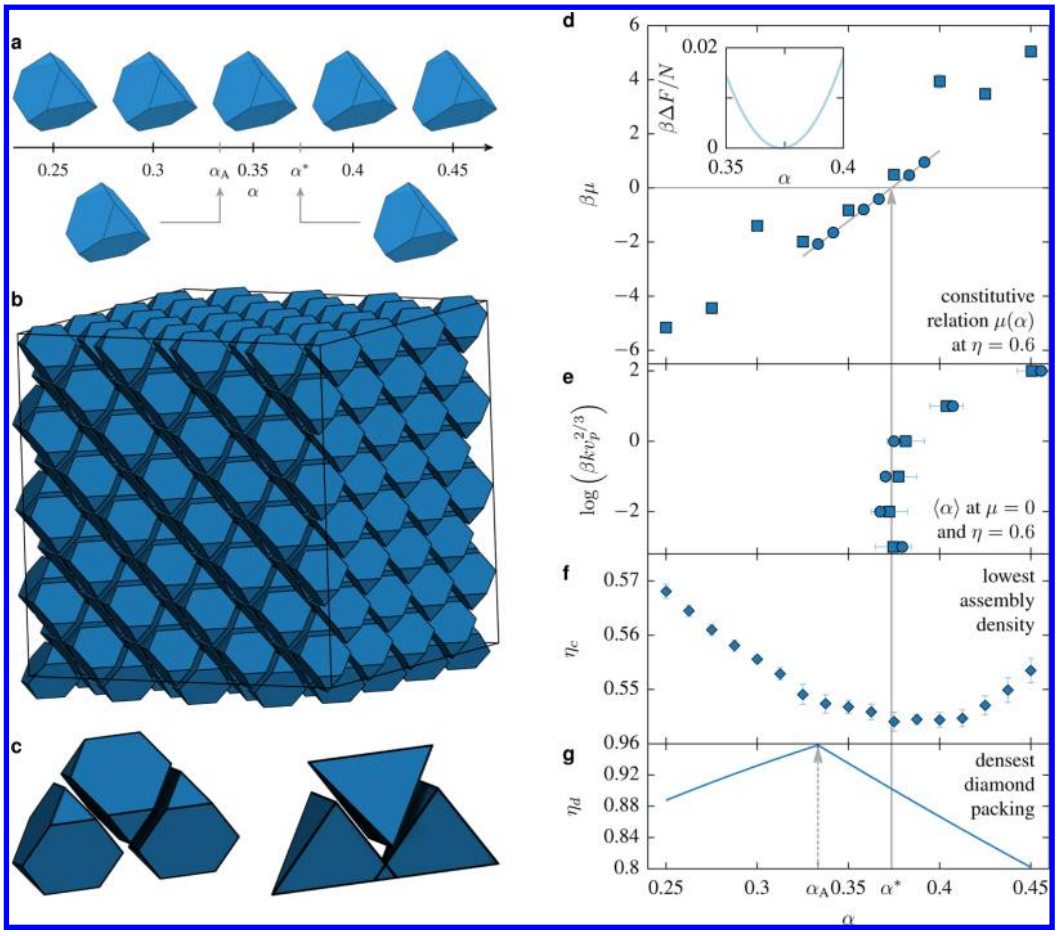

Figure 1. Truncated tetrahedra at a range of truncations α (a) self-assemble a diamond lattice (b).[33] A search for maximal diamond packing density, η_d(*g*), would suggest optimal assembly at $\alpha_A = 1/3$, the Archimedean truncated tetrahedron. We compute the constitutive relation (d) $\mu(\alpha)$ (eq 6) for hard truncated tetrahedra at $\eta = 0.6$. Squares are results for systems with 216 particles, circles for systems with 1000 particles; where visible, error bars are one standard deviation. The alchemical potential vanishes when the truncation is optimal for self-assembling diamond at this density when the truncation is approximately $\alpha^* \approx 0.37$. In the inset plot we reconstruct the free energy curve in the vicinity of the minimum. The increase in anisotropy α^* above the geometric prediction α_A arises because particles need to increase anisotropy to preserve tetrahedral valence at lower packing fractions, but if particles are too anisotropic, the simultaneous coordination of neighboring particles is sterically prohibited (c, see also Figure 2). We demonstrate this design rule (e; see also the SI movie) by simulating tetrahedra with fluctuating shape at $\mu = 0$ in an Einstein crystal with spring constant *k* at packing fraction $\eta = 0.6$ and allowing the particles to find their optimal shape. (e) Plot showing that at low *k* the average truncation $\langle\alpha\rangle$ is consistent with α^* (*N* = 216 squares; *N* = 1000 circles). These findings fall near the minimum of the lowest observed assembly fraction as a function of truncation (f).

adopt a truncation consistent with our alchemical potential calculations at fixed shape. See Figure 1e and the SI movie.

Our computation of the constitutive relation $\mu(\alpha)$ for truncated tetrahedra that form a diamond lattice reveals several findings. (i) By determining that $\mu(\alpha)$ has a root at $\alpha^* \approx 0.37$ we have demonstrated that it is possible to find a thermodynamically optimal shape, among a given family, for self-assembling the diamond lattice. (ii) Our criterion of $\mu(\alpha^*) = 0$ is both parameter-free and independent of system kinetics, which are highly dependent on simulation methods. Nevertheless, we find rough agreement between the thermodynamic computation of the alchemical potential and a measurement of the lower critical packing fraction η_c reported in ref 33, which we reproduce in Figure 1f. (iii) The fact that the optimal particle shape ($\alpha^* \approx 0.37$) for diamond assembly at $\eta = 0.6$ is more tetrahedral than the optimal shape for diamond packing ($\alpha_A = 1/3$), but not perfectly tetrahedral ($\alpha = 1$), arises from a competition between two effects. Particles must have tetrahedral valence to form the diamond lattice, but in the diamond lattice, particles are arranged in an alternating motif (Figure 1c,d). Shape entropy considerations[16] suggest that as the system density is lowered, particles must have larger entropic patches[14] to maintain their emergent valence, as shown in Figure 2. However, as illustrated in Figure 1d, if the particles are too tetrahedral, then the alternating diamond motif leads to overlapping next-to-nearest neighbor particles, as shown in Figure 2. Hence, the optimal truncation of a tetrahedron to self-assemble diamond is more tetrahedral than packing would dictate to preserve valence, but not too tetrahedral

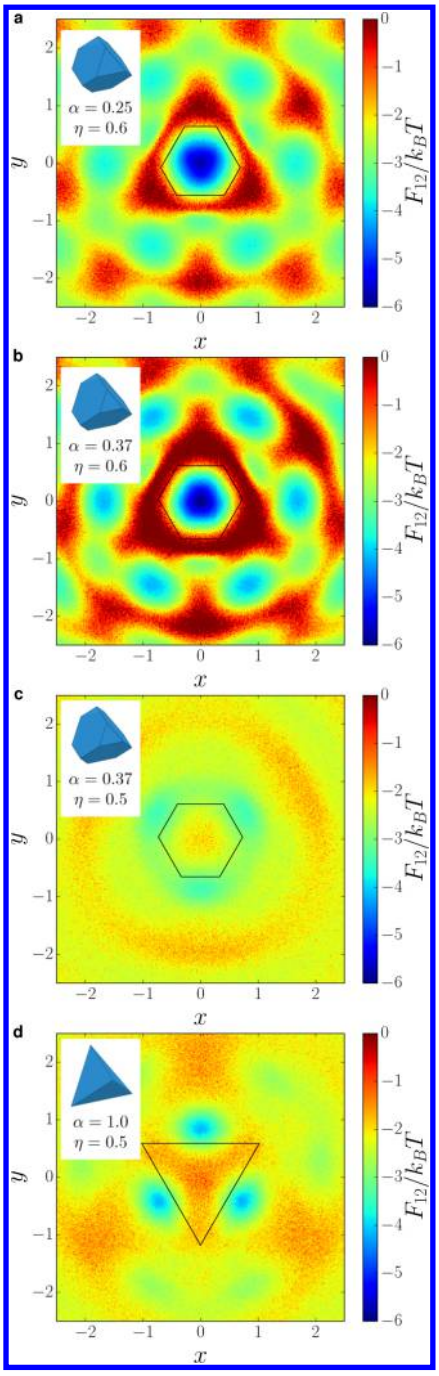

Figure 2. Emergent valence encoded in the PMFT for truncated tetrahedra for a crystal at density $\eta = 0.6$ (a: $\alpha = 0.25$, b: $\alpha = \alpha^* \approx 0.37$) and a fluid at density $\eta = 0.5$ (c: $\alpha = \alpha^* \approx 0.37$, d: $\alpha = 1.0$). In the crystal we see that the particle at the optimal truncation α^* (b) shows greater specificity of tetrahedral valence than at lower α (a), as expected. However, at fluid densities, we see that if the particle is too tetrahedral (d), the second neighbor shell is rotated by $\pi/6$ compared with lower truncations (c) and is incommensurate with the diamond lattice.

to prevent particles from having alternating valence. (iv) We computed the alchemical modulus M_α for truncated tetrahedra at $\eta = 0.6$ and $\alpha = \alpha^*$. In future work it would be interesting to determine how this modulus varies across system density in this system and differs between systems/structures, or relates to effects of polydispersity, and how it behaves at phase boundaries. (v) The entropic assembly of anisotropic hard shapes is driven by emergent valence,[14,16] manifesting in directional entropic forces.[33] A defining feature of emergent behaviors is that their origin is difficult to trace to microscopic attributes of the system constituents.[17] Here, we explicitly demonstrate the general principle that it is possible to optimize building-block attributes, by which we systematically control emergent valence, in order to optimally assemble a target structure. Moreover, our results suggest a general design rule for entropic valence: that as system density decreases, entropic patch size[14] must increase to optimally assemble a dense packing phase. This design rule is supported by another recent result[43] where it was found that for several families of dimpled particles the peak in packing density occurs at an entropic patch size that is below the critical size for the *onset* of entropic assembly at low density. This is particularly strong evidence for the design rule proposed here because the optimal patch size cannot be smaller than the patch size at onset. (vi) In practice, the synthesis of anisotropic colloidal particles is often driven by a growth process that yields particles in a family of shapes. Here we have shown, in an example family, how to optimally choose when to terminate that growth process to obtain particles for assembling a specific target structure.

Rhombic Dodecahedron. To (i) understand how to contrast the relative importance of different shape modifications of a given shape and (ii) determine how this relative importance depends on system density, we studied a two-parameter family of truncations of rhombic dodecahedra that leave them invariant under the spheric triangle group $\Delta_{4,2,3}$.[63] The $\Delta_{4,2,3}$ invariant family of shapes is constructed with three families of planes that make up the faces of a cube, a rhombic dodecahedron, and an octahedron, all oriented to preserve the necessary point group symmetry. The rhombic dodecahedron has two different types of vertices: 4-fold vertices where four planes come together and 3-fold vertices where three planes come together. Moving the planes that make up the faces of the cube toward the origin truncates the 4-fold vertices, and moving the planes that make up the faces of the octahedron truncates the 3-fold vertices. We performed simulations that examine the effects of each type of truncation on a perfect rhombic dodecahedron. We parametrize the vertex truncations so that when $\alpha_4 = 0$ (4-fold vertex truncation) and $\alpha_3 = 0$ (3-fold vertex truncation), the particle is a perfect rhombic dodecahedron. Maximal truncation $\alpha_4 = 1$ and $\alpha_3 = 0$ yields a perfect cube, and $\alpha_4 = 0$ and $\alpha_3 = 1$ yields a perfect octahedron.

We determined how systems of perfect rhombic dodecahedra ($\alpha_4 = \alpha_3 = 0$) respond to infinitesimal

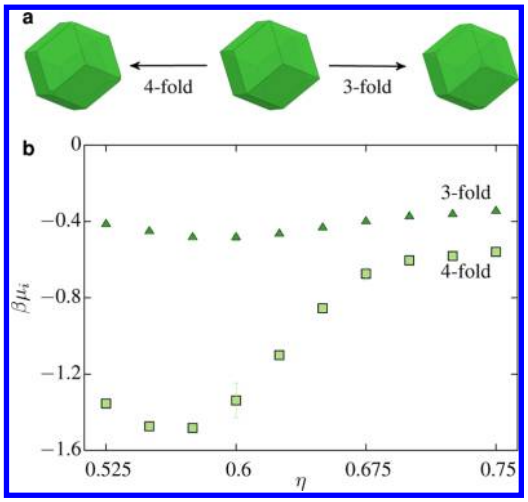

Figure 3. Rhombic dodecahedra have both 4-fold and 3-fold vertices (a). We determine the relative sensitivity to the truncation of each type of vertex by computing the constitutive relation $\mu(\eta)$ (b) according to the (exaggerated) truncations shown in (a). We plot alchemical potentials for 4-fold truncations (μ_4, squares) and 3-fold truncations (μ_3, triangles) at various densities for which the system self-assembles an fcc lattice. We observed $\mu_4 < \mu_3 < 0$ at all densities, indicating that both vertex truncations improve assembly of the target crystal, but 4-fold vertex truncations provide greater improvement.

changes in α_3 and α_4. We computed the alchemical potentials μ_4 conjugate to α_4 (4-fold vertex truncations) and μ_3 conjugate to α_3 (3-fold vertex truncations) for systems of $N = 256$ rhombic dodecahedra at a series of packing densities η between 0.525 and 0.75 in increments of 0.025 at $\alpha_4 = \alpha_3 = 0$. As shown in Figure 3, we find negative alchemical potentials for both 3-fold and 4-fold vertex truncations ($\mu_3, \mu_4 < 0$) at all densities studied, $0.525 \leq \eta \leq 0.75$, implying that both types of vertex truncation *reduce* the free energy of the system. Moreover, we find that truncation of the 4-fold vertices results in a greater reduction in free energy than the 3-fold truncation.

Our computation of the constitutive relations $\mu_i(\eta)$ for rhombic dodecahedra explicitly demonstrates how our methods can determine the relative importance of various shape features. Determining the most important shape features to control is crucial for anisotropic particle synthesis techniques, and here we have demonstrated a general method for solving this problem. In addition to providing this general proof-of-principle, our results have several specific implications. (i) At all densities studied, we observed $\mu_4 < \mu_3 < 0$, indicating that both types of vertex truncation improve the self-assembly of rhombic dodecahedra into a face-centered cubic (fcc) lattice. Because vertex truncation at fixed volume means the particles become slightly more spherical, our result suggests that the structure is further stabilized by particles exchanging some vibrational degrees of freedom for rotational ones. Moreover, (ii) because $\mu_4 < \mu_3$ it suggests that the 4-fold vertex truncations are more important in restricting the rotational motion than the 3-fold vertices. There are eight 3-fold vertices and six 4-fold vertices in a rhombic dodecahedron, but the centroid-to-vertex distance for a 4-fold vertex is 4/3 the distance for a 3-fold vertex. We might suspect that if a vertex type sticks out further from the shape or is greater in number, it will provide a greater steric constraint on the microstates available to the system. Our result that $\mu_4 < \mu_3$ suggests that for the rhombic dodecahedron in an fcc lattice the vertex distance is more important than the number of vertices. It would be interesting to investigate whether this design rule holds for other shapes or is specific to rhombic dodecahedra. (iii) Because the slopes of both $\mu(\eta)$ curves are positive for $\eta \gtrsim 0.6$, it suggests that particles give up rotational entropy faster than translational entropy as the system density increases. We note that the distinction between 4-fold and 3-fold vertices becomes smaller at larger packing fractions, which suggests, surprisingly, that as the particles increasingly lose rotational entropy, the distinction between *how* they lose it becomes *less* important. It would be interesting to see if this result holds more generally in other systems.

Oscillating Pair Potential. To demonstrate that our alchemy approach is not limited to particle shapes, we studied spherical nanoparticles (or point particles) interacting isotropically using a truncated, intermediate range oscillating pair potential studied in ref 42, which is inspired by Friedel oscillations. It can be written in the form

$$U(r) = \frac{\epsilon}{r^{15}} + \frac{\epsilon}{r^3}\cos(k(r - 1.25) - \phi) \qquad (11)$$

This potential has been recently shown to self-assemble an icosahedral quasicrystal for $k_BT = 0.25$ for $0.78 \lesssim k \lesssim 0.82$ and $0.52 \lesssim \phi \lesssim 0.55$.[42] The potential is of particular interest due to the possibility of realizing it in systems of nanoparticles or colloids decorated with appropriate ligands. For these computations, we work in units with $\epsilon = 1$. We performed molecular dynamics (MD) simulations of $N = 4096$ particles using HOOMD-Blue.[64] For full simulation details, see the SI.

We computed the alchemical potentials μ_k conjugate to k (wavenumber) and μ_ϕ conjugate to ϕ (phase shift) for systems of $N = 4096$ particles interacting *via* the oscillating pair potential in eq 11. We studied the pair potential in the range of parameter space that was shown previously[42] to self-assemble an intermediate-density icosahedral quasicrystal. In this phase, we find that within the entire parameter range over which we were able to reliably nucleate the intermediate-density quasicrystal, both μ_k and μ_ϕ are negative. We show this explicitly in Figure 4a, where we form μ_k and μ_ϕ into the vector $\vec{\mu}$. We plot $-\vec{\mu}$, which shows the direction that decreases the free energy at a given point in parameter space.

This result alone does not indicate whether this curious behavior is enthalpic or entropic in origin.

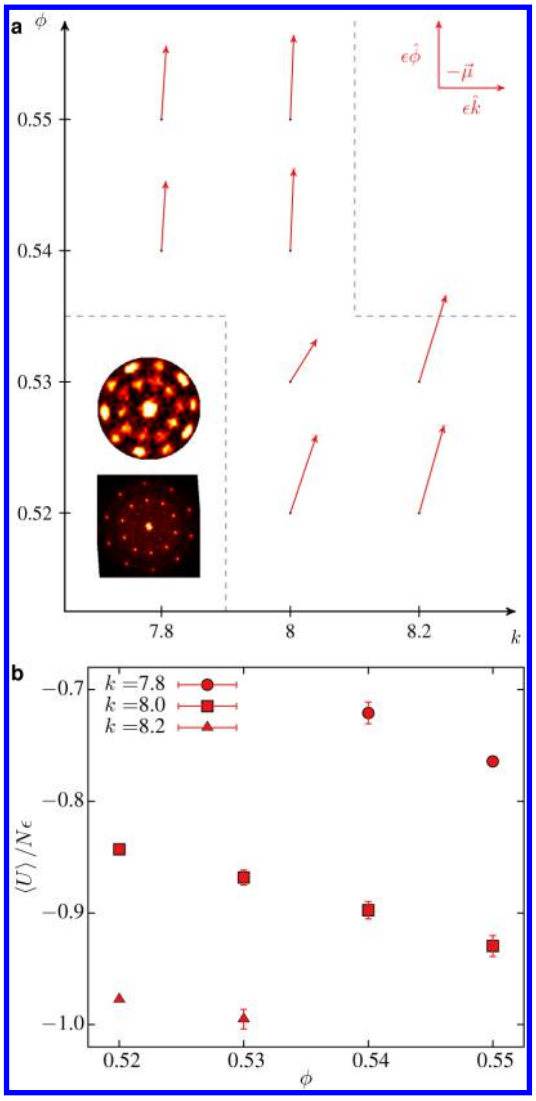

Figure 4. (a) Alchemical potential ($-\vec{\mu}$) for the wavenumber k and phase ϕ parameter in systems of N = 4096 particles interacting *via* a three-well oscillating pair potential over a range of parameters that self-assemble an icosahedral quasicrystal.[42] The pair potential self-assembles icosahedral quasicrystals of three different densities. Here, we examine the region of parameter space that self-assembles the intermediate-density quasicrystal (dashed lines indicate the phase boundaries we observed for the self-assembly of the intermediate-density quasicrystal). Surprisingly, we find that, over the range of parameters we studied, in order to thermodynamically improve the assembly of the intermediate-density quasicrystal, we are driven toward the region of parameter space that is dominated by the self-assembly of the high-density quasicrystalline phase. This suggests that the optimal choice of parameters to stabilize the intermediate-density quasicrystal is buried in a region that will spontaneously self-assemble the high-density phase instead and suggests that the intermediate-density phase will be difficult to stabilize in practice. The insets show the bond order diagram and diffraction pattern from a simulation snapshot of a 4096-particle system at k = 8, ϕ = 0.53. (b) In the same system we computed the average potential energy per particle for different values of k as a function of ϕ. We see a clear decrease in $\langle U\rangle$ with increasing k and ϕ. This finding suggests that the decrease in free energy with increasing k and ϕ shown in panel a can be attributed to enthalpic contributions from lower ground-state energies.

To understand the origin of this decrease in free energy for increasing both k and ϕ, we computed the average potential energy at each state point, which is plotted in Figure 4b. We see that, at a given k, increasing ϕ decreases the system's potential energy and that the potential energy is lower at a given ϕ with increasing k, which is consistent with the alchemical potential results shown in Figure 4a. This suggests that the effect we observe in Figure 4a is enthalpic in origin.

Surprisingly, our result that μ_k and μ_ϕ are everywhere negative suggests that there is not a choice of parameters for which $\vec{\mu} = 0$ (*i.e.*, a local free energy minimum) in the parameter regime where the intermediate-density quasicrystal is the thermodynamically preferred phase. (For an example of a simpler case where there is a local free energy minimum in a system with isotropic interactions, see the SI.) Rather it suggests that, at least for systems of N = 4096 particles, the optimal parameter choice for self-assembling the intermediate-density quasicrystal lies along the boundary separating the assembly of the intermediate-density quasicrystal and the high-density quasicrystal, which is the thermodynamically preferred phase at higher values of k and ϕ.[42]

A general take-away message of ref 42 is that controlling assembly in one-component systems *via* isotropic interaction potentials involves two things. It involves controlling the relative distances of potential energy minima, which determines preferred relative distances between particles. [Note that precise control over this procedure is not straightforward, even at T = 0. See the SI for an explicit demonstration in a toy model system.] However, it also involves controlling the relative depth of the minima, which determines the number of particles that sit at the preferred relative distances determined by the minima locations. Here, we are able to directly compute the effects of changes in potential control parameters on the system free energy, and we find that they can be detected. In the SI, we consider the pattern registration as measured by comparing the locations of the potential minima with the radial distribution function of the particles, and we find no discernible difference across the range of parameters we considered. This suggests that our alchemical potential methods are sensitive to system behavior that is not easily discernible *via* conventional analysis. We believe this might be of particular value in systems such as the oscillating pair potential system where there is a very rich bulk phase structure that depends sensitively on the choice of potential parameters controlling particle valence.[42]

CONCLUSION

We chose families of model systems to demonstrate the power of our methods because of their structural complexity (the icosahedral quasicrystal) or conceptual complexity (the emergent behavior of hard shapes);

however our methods can be generalized straightforwardly to systems of particles with other interactions or shapes, as well as systems with enthalpic patches[7−9] or multiple-particle species. Furthermore, though our focus was on understanding macroscopic colloidal behavior within a given region of phase space, our methods can be applied to the crystallization of other types of matter, *e.g.*, polymers, and the study of phase boundaries. One example where both are relevant is in the investigation of the polymorphism[65] or supramolecular isomerism in crystals of small molecules, which is relevant for pharmaceutical applications.[66]

Here we focused on solving the problem of determining optimal building-block attributes for target structures among a range of building blocks, from which we were able to extract design rules for emergent behavior. As a result, most of our calculations were of the constitutive relation $\mu(N,V,T,\alpha)$. However, for truncated tetrahedra we also considered (Figure 1e and SI Movie) the constitutive relation $\alpha(N,V,T,\mu)$ for particles fixed to sit on a diamond lattice using a simple extension of eq 2 (see the SI for details). All of the foregoing discussion concerning interpretation of alchemical potentials, including the relation to building-block optimality, continues to hold, where any quantities computed in extended ensembles are, by design, conditional on the externally imposed criteria. Using extended ensembles, it is straightforward (see the SI for details) to use our techniques for the discovery of building blocks for bulk materials given a suitable choice of external design criteria. We leave a full numerical investigation of this class of problems to future work.

Our method for determining optimal building blocks to self-assemble target structures was based on the desire to make quantitative connections between building-block attributes and bulk behavior. To make our proof-of-principle demonstration explicit, we ensured that the local minima we identified were *bona fide* global minima by computing exhaustively over relevant building-block attributes. Rather than computing exhaustively as we have here, future investigations should reduce computational effort by employing global optimization techniques. Indeed, work aimed at optimizing building blocks for bulk attributes has employed genetic or evolutionary algorithms[67−71] or gradient descent.[72] Those approaches are complementary to the optimization part of the present work in three ways: (i) Our approach provides a systematic, rigorous, first-principles method for constructing probability distributions needed to apply the gradient descent method proposed in ref 72. (ii) Genetic and evolutionary algorithms are powerful techniques that use external fitness criteria to perform nonlocal optimization. Our approach supplements these nonlocal approaches by providing direct, precise measurement of the physical response of a system to a local change in the attributes of building blocks. (iii) The ability to probe local changes in building-block attributes is also important because, in addition to optimizing attributes, we would like to be able to derive generalizable design rules that extend beyond specific systems of interest. Here we showed an example of how to develop general design rules using digital alchemy by showing that dense packing arguments for anisotropic shapes can be extended to lower density by increasing the size of entropic patches. Although this result and our examples concerned colloidal systems, there is nothing that precludes the immediate extension of our techniques to materials made of any type of building blocks that have adjustable interactions. We believe that a combination of the methods we present here with existing techniques[67−70,72] will provide a powerful tool set for materials design.

Although the periodic table has many functions, for materials scientists it provides a useful, complete heuristic for anticipating the bulk behavior of atomic elements, based on atomic valence. A similar construct for colloids that gives a complete, heuristic tabulation of relationships between building-block attributes *vs* bulk structures would be desirable. However, in systematically classifying particles, refs 8 and 14 showed that particle valence can be described simultaneously along several orthogonal anisotropy dimensions. The intrinsically high dimensionality of this classification means that any set of relationships between building block attributes and bulk structure for colloids, unlike those in the periodic table, cannot be complete. Nevertheless, work on enthalpically[7,8] and entropically[14] patchy particles has shown that projecting key structural features onto constituent particles, *via* anisotropy dimensions, yields heuristic relationships between building-block attributes and bulk structure. Here, we showed that these relationships can be made quantitative so that desired building-block attributes can be precisely engineered. In summary, whereas the building block *vs* bulk relationships predicted by the periodic table are complete but heuristic, building block *vs* bulk relationships for colloids are necessarily incomplete, but are quantitative in a way that we have shown here both provides general intuition and opens the possibility of designing optimal building blocks.

Finally, we showed how to directly compute alchemical response functions using numerical calculations on model systems, but it is also interesting to speculate how they might be measured in some example experimental systems. Some experimental systems have anisotropic colloidal particles that change their effective shape depending on the density of adsorbed surface ligands.[31,56,57] In systems where the adsorption of surface ligands is reversible, one can imagine that the density or distribution of adsorption depends on the

TABLE 1. Contrast between Constraints on Engineering Materials with Atomic Elements and Colloidal "Elements"[a]

	atomic matter	colloidal matter
anisotropy dimensions	proton number	many
anisotropy dimension types	discrete	discrete, continuous
valence constraints	quantum mechanics, group theory, Fermi statistics	steric
number of stable elements	~80	infinite

[a] Colloidal elements have valence that can vary continuously in many different ways. The malleability of colloid valence means that constructing a "periodic table" for them is inherently difficult. However, we can exploit the malleability of colloids to directly probe how particle attributes affect structure.

macroscopic phase the particles are in. For example, ligand adsorption frequently leads to particles becoming effectively more spherical.[31] Imagine taking spheroidal particles and organizing them into a non-close-packed lattice. We would expect some ligands to desorb from the particle surface to make the particles less spherical so that they can accommodate the lattice structure they are in. Measuring particle shape (or the change in the reservoir concentration of ligands) for particles in the bulk structure, one could directly (indirectly) measure how particle anisotropy is affected by bulk structure through $\alpha(\mu = 0)$ and χ_α. In contrast, to measure the alchemical potential, one could increase the ligand reservoir concentration so that an above-optimal density of ligands adsorbs on the particle surface and then determine the free energy required to further increase adsorption. As another example, in colloidal amphiphile or Janus particle systems, effective patch size is determined by salt concentration.[44] One could imagine that if Janus particles are fabricated to self-assemble a structure but have suboptimal patch size, the system could lower its overall free energy by locally altering the salt concentration near the Janus particles so that the effective patch size is closer to the optimal one. Detecting such an effect experimentally could involve measuring differences in reservoir salt concentration between self-assembled and disordered systems.

METHODS

To compute alchemical potentials we used standard MC simulations (for truncated tetrahedra and rhombic dodecahedra; see, for example, ref 61) or MD simulations performed with HOOMD-Blue (for the oscillating pair potential; see ref 64) to sample the equilibrium distribution of configurations for particles with given attributes in a given structure. We compared series of configurations for particles of attributes $\{\alpha_i\}$ to configurations of particles with perturbed attributes $\{\alpha_i'\}$, and *vice versa*, using the Bennett acceptance ratio method[53] and an appropriately chosen finite differencing scheme[73] to extract the alchemical potential. Full details, including the analysis of statistical and systematic errors, can be found in the SI.

Simulations of fluctuating shape at fixed alchemical potential were performed with HPMC,[74] an in-house HOOMD-Blue[64] plugin for hard particle MC simulations. In addition to standard MC moves, particles were confined to an Einstein crystal lattice and subjected to collective trial moves on their shape. Full simulation details and a discussion of detailed balance for ensembles with fluctuating particle attributes can be found in the SI. Lowest assembly fractions were computed from 10 independent simulations of 2000 particles at a series of packing fractions at each truncation.

Conflict of Interest: The authors declare no competing financial interest.

Acknowledgment. We thank K. Ahmed, J. Anderson, D. Beltrán-Villegas, J. Crocker, E. Eiser, D. Frenkel, O. Gang, L. Isa, D. Kofke, I. Kretzschmar, R. Newman, B. Schultz, K. Stebe, A. Sweeney, and J. Swift for helpful discussions and encouragement; C. Phillips for discussions and providing simulation code for the Lennard-Jones-Gauss system; M. Engel for providing simulation code for the polyhedra; J. Antonaglia for a careful reading of an early version of the manuscript; J. Dshemuchadse for helpful discussions and comments on the manuscript; P. Damasceno for helpful discussions, encouragement, and assistance with structure identification; and H. Jaeger for generously sharing a prepublication version of ref 72. This material is based upon work supported in part by the U.S. Army Research Office under Grant Award No. W911NF-10-1-0518 and the U.S. Department of Energy, Office of Basic Energy Sciences, Division of Materials Sciences and Engineering, under Award DE-FG02-02ER46000. P.D. was supported by the National Science Foundation, Emerging Frontiers in Research and Innovation Award EFRI-1240264. D.K. acknowledges funding by the FP7Marie Curie Actions of the European Commission, Grant Agreement PIOF-GA-2011-302490 Actsa. Computational resources and services were supported by Advanced Research Computing at the University of Michigan, Ann Arbor.

Supporting Information Available: The Supporting Information is available free of charge on the ACS Publications website at DOI: 10.1021/acsnano.5b04181.

Full simulation details (PDF)
Movie (MP4)

REFERENCES AND NOTES

1. Mendelejeff, D. Zur Frage über das System der Elemente. *Ber. Dtsch. Chem. Ges.* **1871**, *4*, 348–352.
2. Mendeleeff The Periodic Law of the Chemical Elements. *J. Chem. Soc., Trans.* **1889**, *55*, 634–656.
3. Lewis, G. N. The Atom and the Molecule. *J. Am. Chem. Soc.* **1916**, *38*, 762–785.
4. Holmyard, E. J. *Makers of Chemistry*; Oxford: Oxford, 1931.
5. Perrier, C.; Segré, E. Some Chemical Properties of Element 43. *J. Chem. Phys.* **1937**, *5*, 712–716.
6. Perrier, C.; Segré, E. Technetium: The Element of Atomic Number 43. *Nature* **1947**, *159*, 24.
7. Zhang, Z.; Glotzer, S. C. Self-Assembly of Patchy Particles. *Nano Lett.* **2004**, *4*, 1407–1413.
8. Glotzer, S. C.; Solomon, M. J. Anisotropy of Building Blocks and Their Assembly Into Complex Structures. *Nat. Mater.* **2007**, *6*, 557–562.
9. Pawar, A. B.; Kretzschmar, I. Fabrication, Assembly, and Application of Patchy Particles. *Macromol. Rapid Commun.* **2010**, *31*, 150–168.
10. Sacanna, S.; Pine, D. J. Shape-Anisotropic Colloids: Building Blocks for Complex Assemblies. *Curr. Opin. Colloid Interface Sci.* **2011**, *16*, 96–105.
11. Zhang, G.; Wang, D.; Möhwald, H. Decoration of Microspheres with Gold Nanodots-Giving Colloidal Spheres Valences. *Angew. Chem., Int. Ed.* **2005**, *44*, 7767–7770.
12. Kraft, D. J.; Groenewold, J.; Kegel, W. K. Colloidal Molecules with Well-Controlled Bond Angles. *Soft Matter* **2009**, *5*, 3823–3826.

13. Wang, Y.; Wang, Y.; Breed, D. R.; Manoharan, V. N.; Feng, L.; Hollingsworth, A. D.; Weck, M.; Pine, D. J. Colloids with Valence and Specific Directional Bonding. *Nature* **2012**, *491*, 51–55.
14. van Anders, G.; Ahmed, N. K.; Smith, R.; Engel, M.; Glotzer, S. C. Entropically Patchy Particles: Engineering Valence through Shape Entropy. *ACS Nano* **2014**, *8*, 931–940.
15. Lu, F.; Yager, K. G.; Zhang, Y.; Xin, H.; Gang, O. Superlattices Assembled Through Shape-Induced Directional Binding. *Nat. Commun.* **2015**, *6*, 6912.
16. van Anders, G.; Klotsa, D.; Ahmed, N. K.; Engel, M.; Glotzer, S. C. Understanding Shape Entropy Through Local Dense Packing. *Proc. Natl. Acad. Sci. U. S. A.* **2014**, *111*, E4812–E4821.
17. Anderson, P. W. More Is Different. *Science* **1972**, *177*, 393–396.
18. Sandhage, K. H. Materials "Alchemy": Shape-Preserving Chemical Transformation of Micro-to-Macroscopic 3-D Structures. *JOM* **2010**, *62*, 32–43.
19. Teter, D. M. Computational Alchemy: The Search for New Superhard Materials. *MRS Bull.* **1998**, *23*, 22–27.
20. Paliwal, H.; Shirts, M. R. A Benchmark Test Set for Alchemical Free Energy Transformations and Its Use to Quantify Error in Common Free Energy Methods. *J. Chem. Theory Comput.* **2011**, *7*, 4115–4134.
21. Batista, V. M. O.; Miller, M. A. Crystallization of Deformable Spherical Colloids. *Phys. Rev. Lett.* **2010**, *105*, 088305.
22. Dzugutov, M. Glass Formation in a Simple Monatomic Liquid with Icosahedral Inherent Local Order. *Phys. Rev. A: At., Mol., Opt. Phys.* **1992**, *46*, R2984–R2987.
23. Dijkstra, M.; van Roij, R. Entropy-Driven Demixing in Binary Hard-Core Mixtures: From Hard Spherocylinders Towards Hard Spheres. *Phys. Rev. E: Stat. Phys., Plasmas, Fluids, Relat. Interdiscip. Top.* **1997**, *56*, 5594–5602.
24. Engel, M.; Trebin, H.-R. Self-Assembly of Monatomic Complex Crystals and Quasicrystals with a Double-Well Interaction Potential. *Phys. Rev. Lett.* **2007**, *98*, 225505.
25. Phillips, C. L.; Voth, G. A. Discovering Crystals Using Shape Matching and Machine Learning. *Soft Matter* **2013**, *9*, 8552–8568.
26. Sacanna, S.; Irvine, W. T. M.; Chaikin, P. M.; Pine, D. Lock and Key Colloids. *Nature* **2010**, *464*, 575–578.
27. Marechal, M.; Kortschot, R. J.; Demirörs, A. F.; Imhof, A.; Dijkstra, M. Phase Behavior and Structure of a New Colloidal Model System of Bowl-Shaped Particles. *Nano Lett.* **2010**, *10*, 1907–1911.
28. Marechal, M.; Dijkstra, M. Phase Behavior and Structure of Colloidal Bowl-Shaped Particles: Simulations. *Phys. Rev. E* **2010**, *82*, 031405.
29. de Graaf, J.; van Roij, R.; Dijkstra, M. Dense Regular Packings of Irregular Nonconvex Particles. *Phys. Rev. Lett.* **2011**, *107*, 155501.
30. Rossi, L.; Sacanna, S.; Irvine, W. T. M.; Chaikin, P. M.; Pine, D. J.; Philipse, A. P. Cubic Crystals from Cubic Colloids. *Soft Matter* **2011**, *7*, 4139–4142.
31. Zhang, Y.; Lu, F.; van der Lelie, D.; Gang, O. Continuous Phase Transformation in Nanocube Assemblies. *Phys. Rev. Lett.* **2011**, *107*, 135701.
32. Kraft, D. J.; Ni, R.; Smallenburg, F.; Hermes, M.; Yoon, K.; Weitz, D. A.; van Blaaderen, A.; Groenewold, J.; Dijkstra, M.; Kegel, W. K. Surface Roughness Directed Self-Assembly of Patchy Particles into Colloidal Micelles. *Proc. Natl. Acad. Sci. U. S. A.* **2012**, *109*, 10787–10792.
33. Damasceno, P. F.; Engel, M.; Glotzer, S. C. Crystalline Assemblies and Densest Packings of a Family of Truncated Tetrahedra and the Role of Directional Entropic Forces. *ACS Nano* **2012**, *6*, 609–614.
34. Ni, R.; Gantapara, A. P.; de Graaf, J.; van Roij, R.; Dijkstra, M. Phase Diagram of Colloidal Hard Superballs: from Cubes *via* Spheres to Octahedra. *Soft Matter* **2012**, *8*, 8826–8834.
35. Damasceno, P. F.; Engel, M.; Glotzer, S. C. Predictive Self-Assembly of Polyhedra into Complex Structures. *Science* **2012**, *337*, 453–457.
36. Sacanna, S.; Korpics, M.; Rodriguez, K.; Colon-Melendez, L.; Kim, S.-H.; Pine, D. J.; Yi, G.-R. Shaping Colloids for Self-Assembly. *Nat. Commun.* **2013**, *4*, 1688.
37. Gantapara, A. P.; de Graaf, J.; van Roij, R.; Dijkstra, M. Phase Diagram and Structural Diversity of a Family of Truncated Cubes: Degenerate Close-Packed Structures and Vacancy-Rich States. *Phys. Rev. Lett.* **2013**, *111*, 015501.
38. Jain, A.; Errington, J. R.; Truskett, T. M. Inverse Design of Simple Pairwise Interactions with Low-Coordinated 3D Lattice Ground States. *Soft Matter* **2013**, *9*, 3866–3870.
39. Wang, Y.; Wang, Y.; Zheng, X.; Yi, G.-R.; Sacanna, S.; Pine, D. J.; Weck, M. Three-Dimensional Lock and Key Colloids. *J. Am. Chem. Soc.* **2014**, *136*, 6866–6869.
40. Kim, S.-H.; Hollingsworth, A. D.; Sacanna, S.; Chang, S.-J.; Lee, G.; Pine, D. J.; Yi, G.-R. Synthesis and Assembly of Colloidal Particles with Sticky Dimples. *J. Am. Chem. Soc.* **2012**, *134*, 16115–16118.
41. Millan, J. A.; Ortiz, D.; Glotzer, S. C. Effect of Shape on the Self-Assembly of Faceted Patchy Nanoplates with Irregular Shape into Tiling Patterns. *Soft Matter* **2015**, *11*, 1386–1396.
42. Engel, M.; Damasceno, P. F.; Phillips, C. L.; Glotzer, S. C. Computational Self-Assembly of a One-Component Icosahedral Quasicrystal. *Nat. Mater.* **2014**, *14*, 109–116.
43. Ahmed, N. K.; van Anders, G.; Chen, E. R.; Glotzer, S. C. Crossover Behavior in the Packing and Assembly of Concave Building Blocks. *arXiv*: 1501.03130 [cond-mat.mtrl-sci], **2015**.
44. Zhang, J.; Luijten, E.; Granick, S. Toward Design Rules of Directional Janus Colloidal Assembly. *Annu. Rev. Phys. Chem.* **2015**, *66*, 581–600.
45. Harper, E. S.; Marson, R. L.; Anderson, J. A.; van Anders, G.; Glotzer, S. C. Shape Allophiles Improve Entropic Assembly. *Soft Matter* **2015**, *11*, 7250–7256.
46. Haber, H. E.; Weldon, H. A. Finite-Temperature Symmetry Breaking as Bose−Einstein Condensation. *Phys. Rev. D: Part. Fields* **1982**, *25*, 502–525.
47. Yamada, D.; Yaffe, L. G. Phase Diagram of N = 4 Super-Yang-Mills Theory with R-Symmetry Chemical Potentials. *J. High Energy Phys.* **2006**, *0609*, 027.
48. Shannon, C. A. Mathematical Theory of Communication. *Bell Syst. Tech. J.* **1948**, *27*, 379–423.
49. Jaynes, E. T. Information Theory and Statistical Mechanics. *Phys. Rev.* **1957**, *106*, 620–630.
50. Shieh, H.-H.; van Anders, G.; Van Raamsdonk, M. Coarse-Graining the Lin-Maldacena Geometries. *J. High Energy Phys.* **2007**, *0709*, 059.
51. Jiang, Q.-Q.; Wu, S.-Q.; Cai, X. Hawking Radiation from the (2 + 1)-Dimensional BTZ Black Holes. *Phys. Lett. B* **2007**, *B651*, 58–64.
52. Maeda, K.; Natsuume, M.; Okamura, T. Viscosity of Gauge Theory Plasma with a Chemical Potential from AdS/CFT. *Phys. Rev.* **2006**, *D73*, 066013.
53. Bennett, C. H. Efficient Estimation of Free Energy Differences From Monte Carlo Data. *J. Comput. Phys.* **1976**, *22*, 245–268.
54. Landau, L. D.; Lifshitz, E. M. *Statistical Physics, Part 1*, 3rd ed.; Butterworth-Heinemann: Oxford, 1980.
55. Landau, L. D.; Lifshitz, E. M. *Theory of Elasticity*, 3rd ed.; Butterworth-Heinemann: Oxford, 1986.
56. Gang, O.; Zhang, Y. Shaping Phases by Phasing Shapes. *ACS Nano* **2011**, *5*, 8459–8465.
57. Ye, X.; Jun, C.; Engel, M.; Millan, J. A.; Li, W.; Qi, L.; Xing, G.; Collins, J. E.; Kagan, C. R.; Li, J.; et al. Competition of Shape and Interaction Patchiness for Self-Assembling Nanoplates. *Nat. Chem.* **2013**, *5*, 466–473.
58. Kamien, R. D. In *Soft Matter, Vol. 3, Colloidal Order: Entropic and Surface Forces*; Gompper, G., Schick, M., Eds.; Wiley-VCH: Weinheim, 2007; Chapter 1, pp 1−40.
59. Escobedo, F. A. Engineering Entropy in Soft Matter: the Bad, the Ugly and the Good. *Soft Matter* **2014**, *10*, 8388–8400.
60. Frenkel, D. Order through Entropy. *Nat. Mater.* **2014**, *14*, 9–12.
61. Haji-Akbari, A.; Engel, M.; Keys, A. S.; Zheng, X.; Petschek, R. G.; Palffy-Muhoray, P.; Glotzer, S. C. Disordered,

Quasicrystalline and Crystalline Phases of Densely Packed Tetrahedra. *Nature* **2009**, *462*, 773–777.
62. Gilbert, E.; Johnson, D.; Keerthi, S. A Fast Procedure for Computing the Distance between Complex Objects in Three-Dimensional Space. *IEEE J. Robotics and Automation* **1988**, *4*, 193–203.
63. Chen, E. R.; Klotsa, D.; Engel, M.; Damasceno, P. F.; Glotzer, S. C. Complexity in Surfaces of Densest Packings for Families of Polyhedra. *Phys. Rev. X* **2014**, *4*, 011024.
64. Anderson, J. A.; Glotzer, S. C. The Development and Expansion of HOOMD-Blue through Six Years of GPU Proliferation. *arXiv*: 1308.5587 [physics.comp-ph] 2013, http://codeblue.umich.edu/hoomd-blue.
65. Wöhler; Liebig Untersuchungen über das Radikal der Benzoesäure. *Ann. Pharm. (Lemgo, Ger.)* **1832**, *3*, 249–282.
66. Moulton, B.; Zaworotko, M. J. From Molecules to Crystal Engineering: Supramolecular Isomerism and Polymorphism in Network Solids. *Chem. Rev.* **2001**, *101*, 1629–1658.
67. Venkatasubramanian, V.; Chan, K.; Caruthers, J. Computer-Aided Molecular Design Using Genetic Algorithms. *Comput. Chem. Eng.* **1994**, *18*, 833–844.
68. Miskin, M. Z.; Jaeger, H. M. Adapting Granular Materials Through Artificial Evolution. *Nat. Mater.* **2013**, *12*, 326–331.
69. Srinivasan, B.; Vo, T.; Zhang, Y.; Gang, O.; Kumar, S.; Venkatasubramanian, V. Designing DNA-Grafted Particles that Self-Assemble into Desired Crystalline Structures Using the Genetic Algorithm. *Proc. Natl. Acad. Sci. U. S. A.* **2013**, *110*, 18431–18435.
70. Miskin, M. Z.; Jaeger, H. M. Evolving Design Rules for the Inverse Granular Packing Problem. *Soft Matter* **2014**, *10*, 3708–3715.
71. Geng, Y.; Damasceno, P. F.; Glotzer, S. C. *Preprint*, **2015**.
72. Miskin, M. Z.; de Pablo, J. J.; Jaeger, H. M. Turning Statistical Physics Models Into Materials Design Engines. *Preprint*, **2015**.
73. Fornberg, B. Generation of Finite Difference Formulas on Arbitrarily Spaced Grids. *Mathematics of Computation* **1988**, *51*, 699–706.
74. Anderson, J. A.; Jankowski, E.; Grubb, T. L.; Engel, M.; Glotzer, S. C. Massively Parallel Monte Carlo for Many-Particle Simulations on GPUs. *J. Comput. Phys.* **2013**, *254*, 27–38.